Formation of a transient Si hydride multilayer and recrystallization of a Si-Si network during vacuum-ultraviolet-excited Si homoepitaxy from Si_2H_6

Housei Akazawa
NTT System Electronics Laboratories, 3-1 Morinosato Wakamiya, Atsugi-shi, Kanagawa 243-01, Japan
(Received 1 June 1998; revised manuscript received 27 August 1998)

The mechanism of vacuum-ultraviolet-excited Si epitaxy on Si(100) from Si_2H_6 has been clarified by spectroellipsometric measurement. The crystallinity evolution, classified into three types which depend strongly on the photon flux, is discriminated by distinct shapes of (Ψ,Δ) trajectories. The formation of a Si hydride multilayer at the outermost surface was evidenced by the immediate changes in the (Ψ,Δ) angles when Si_2H_6 is introduced. This layer is decomposed quickly when the Si_2H_6 supply is terminated. The Si hydride layer is then converted into a crystalline Si-Si network involving voids due to the photon-stimulated desorption of H atoms. For the epitaxy is to be maintained, the vacuum-ultraviolet-stimulated rearrangement of the Si-Si network into a dense Si crystal must further occur at a higher rate than deposition of Si hydrides. [S0163-1829(99)02604-1]

I. INTRODUCTION

Synchrotron-radiation-excited chemical-vapor deposition (SR-CVD), a growth technique which allows low-temperature epitaxy with angstrom-order controllability of film thickness, has recently been used to grow Si films from Si_2H_6 (Refs. 1–3) and Ge films from GeH_4 (Refs. 3 and 4). The kinetic pathways of Si-atom deposition include photolysis of Si_2H_6 molecules, reactive sticking of the photodecomposed fragments, regeneration of dangling bonds by direct abstraction of H by an impinging H atom, or by photon-stimulated desorption (PSD) of H atoms.[2] Although these processes have been identified experimentally, we still do not know how the Si admolecules introduced at the surface are eventually incorporated into the bulk Si crystal network nor why epitaxy is maintained at temperatures as low as 230 °C.[1] Akazawa and Utsumi[2] proposed the following sequential conversion scheme:

$$\mathrm{SiH}_x(g) \rightarrow m\mathrm{SiH}_x(a) \rightarrow (\text{-}\mathrm{SiH}_x\text{-}) \rightarrow \text{Si crystal}, \qquad (1)$$

where $\mathrm{SiH}_x(g)$ denotes photolysis products in the ambient, $m\mathrm{SiH}_x(a)$ is a silicon hydride multilayer or aggregate formed at the outermost surface, and $(\text{-}\mathrm{SiH}_x\text{-})$ is the infant stage of a Si-Si network eventually converted into crystalline Si (c-Si). The work described in the present paper confirmed the proposed scheme by using ultraviolet spectroscopic ellipsometry (SE) as an analytical method.

The existence of the $m\mathrm{SiH}_x(a)$ layer was originally inferred from the fact that the activation energies and the growth rates differ substantially between parallel and perpendicular incidence of SR. The higher growth rate at perpendicular incidence was interpreted as indicating that an additional excitation mechanism due to secondary electrons enhanced the formation of $m\mathrm{SiH}_x(a)$ and the conversion of $m\mathrm{SiH}_x(a)$ to $(\text{-}\mathrm{SiH}_x\text{-})$.[1,2] When the dielectric function of the overlayer differs from that of the underlying substrate, SE can sensitively monitor the changes in the composition, crystallinity, and surface roughness of the growing material. The immediate formation and decomposition processes of $m\mathrm{SiH}_x(a)$ layer at the outermost surface have been verified by kinetic monitoring of the dielectric response change. The second new content of the present work is its evidence for the formation of $(\text{-}\mathrm{SiH}_x\text{-})$. The dielectric response of $(\text{-}\mathrm{SiH}_x\text{-})$ is characterized by vacancies in the network, while that of $m\mathrm{SiH}_x(a)$ is characterized by Si-H bonds. It was found that these two intermediate states can be discriminated by their different dielectric functions.

Another content is relevant to the conversion of $(\text{-}\mathrm{SiH}_x\text{-})$ to the Si crystal. The vacuum-ultraviolet (vuv)-stimulated crystallization of a Si-Si network has already been reported.[5–7] In the present work this process has been investigated in detail by changing the growth parameters during the steady-state SR-CVD growth and by post-irradiating an amorphouslike overlayer with an intense vuv beam. Amorphous Si (a-Si) is metastable with respect to c-Si. Once exchange of chemical bonds and rearrangement of Si-atom positions are triggered, crystallization can proceed continuously if all the heat released is used for advancing the a-Si/c-Si interface. This happens when recrystallization is initiated by a high-power excimer laser pulse[8] that actually melts the a-Si layer.[9] The photon flux from synchrotron radiation in a pulse is much lower than that delivered by excimer lasers. Hence vuv-stimulated crystallization occurs under microscopically hot but macroscopically frozen conditions specific to core electronic excitation. We discuss how the breaking of Si-H and Si-Si bonds contributes to restructuring the network and recrystallization.

II. EXPERIMENT

The growth experiments were performed using beamline 7 on the compact electron storage ring ''Super-ALIS'' at the NTT Atsugi Research and Development Center. The beamline components, the growth chamber at the end station, and the gas feeding and exhausting systems are described elsewhere.[10] Briefly, synchrotron radiation emitted at the superconducting bending magnet is focused by two toroidal mirrors onto the surface of a specimen mounted in an

ultrahigh-vacuum chamber (base pressure 5×10^{-10} Torr). The energy of photons delivered ranges from 10 to 1500 eV, and the maximum flux is at 100 eV. During the 5.5-h interval between the electron injection times the storage ring current (I_R) fell from 470 to 250 mA. Correspondingly, the photon flux density at the specimen surface was between 1.1 and $0.6\times10^{16}\,s^{-1}\,mm^{-2}$.

The reactant gas was 99.99% pure Si_2H_6, and the substrates were rectangular pieces ($14\times19\,mm^2$) of silicon wafers oriented toward the (100) direction. Before the substrate specimens were put into the chamber, they were pretreated by dipping them for 20 s in a 2.5% solution of hydrofluoric acid. According to the literature,[11] this leaves the surface significantly rough and terminated predominantly by various silicon hydrides. In some experiments the HF-treated Si(100) specimens were used as is, but unless otherwise stated the SR-CVD growth was performed after a Si buffer layer (about 60 nm thick) had been grown on the HF-treated surface by Si_2H_6 gas-source molecular-beam epitaxy (GSMBE). The growth temperature for the buffer layer growth was 600 °C and the Si_2H_6 pressure was 5×10^{-4} Torr. The thermal and SR-CVD growth rates were evaluated from some cross-sectional transmission electron microscopy (XTEM) images of thick Si films.

SE measures the ratio ρ between the complex reflection coefficients (r_p and r_s) of *p*- and *s*-polarized light incident to the solid surface. The ellipsometric angles Ψ and Δ, corresponding, respectively, to the amplitude and the phase of ρ are defined by the relation $\rho=r_p/r_s=\tan\Psi\exp(i\Delta)$. The pseudodielectric function $\langle\varepsilon\rangle$ is calculated from these angles by using the relation $\langle\varepsilon\rangle=\sin^2\phi+\sin^2\phi\,\tan^2\phi(1-\rho)^2/(1+\rho)^2$, where ϕ is the incident angle of the probe light. Although SE is generally sensitive to the state of material near the surface of a film, its sensitivity to the outermost surface is lower than the other surface-specific analytical tools. Thus the most suitable application of SE is to the monitoring and control of nanometer-scale material processing. If the overlayer film is homogeneous, and optical constants of the elemental phases are known, its thickness and composition can be determined precisely using the Bruggeman effective-medium approximation.

The SE optics we employed was the phase-modulation-type.[12] This detection technique is appropriate for kinetic measurement of vuv-excited reactions at high speed: Because the standard clock frequency for operation (125 MHz) of the synchrotron is far higher than the frequency of the photoelastic modulator (50 kHz), the vuv beam can be regarded a direct current. Irradiation with the quasidirect current vuv beam therefore does not interfere with the phase-modulated determination of ellipsometric angles. If the diffusion and recombination of photoexcited carriers significantly change the dielectric properties of the material, these factors could modify the (Ψ,Δ) values.[13]

The vuv beam illuminated the specimen surface at an angle 12° from the surface normal, and the UV probe light for SE illuminated the surface at an angle 72° from the surface normal. Birefringings were avoided by using stress-free quartz viewports in the optical path of the UV beam. The rectangular vuv-irradiated area measured $10\times18\,mm^2$. The sampling region of the SE signal was elliptical, with major and minor axes of 10 and 3 mm, and was centered within the rectangular vuv-irradiated area. Static SE spectra were measured before and after growth, both at the growth temperature and when the sample was cooled to room temperature after a series of growth. The energy range was from 1.5 to 5 eV, in 0.05-eV intervals. Kinetic SE data during SR-CVD were obtained at a fixed photon energy of 3.4 eV, with data sampling every 10 s.

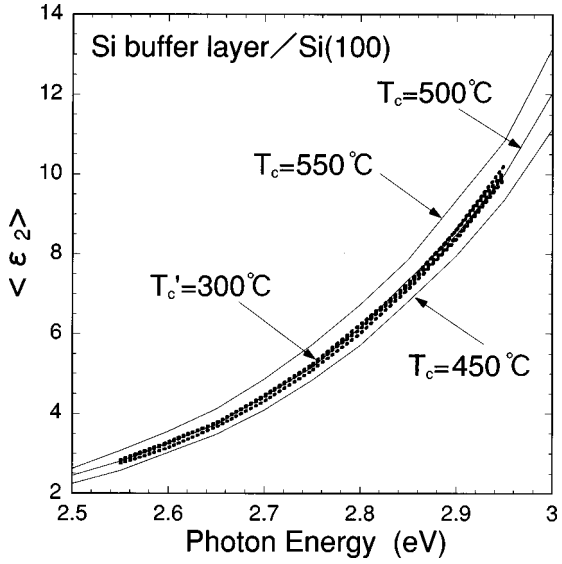

FIG. 1. Comparison of the $\langle\varepsilon_2\rangle$ spectrum of HF-etched Si(100) for the calibration of the surface temperature. The three solid curves were obtained only by heater annealing, and the dotted curves were obtained under vuv irradiation at 430, 400, 350, and 290 mA of storage current, while using additional annealing to keep $T_c'=300\,°C$.

The temperature of the wafer surface was calibrated carefully. The temperature monitored by a thermocouple in contact with the backside of the wafer is denoted T_c, and the real temperature at the front surface is denoted T_s. When the wafer was annealed at $T_c\sim400\,°C$ using a carbon heater from the backside, the relation $T_s=T_c-120\,°C$ was satisfied, which was derived by extrapolating the relation of T_c between 600 and 800 °C with respect to the T_s measured by an optical pyrometer. The temperature gradient between the front and back sides of the wafer was due to dissipation of the heat radiatively into space and conductively to the sample holder. When the wafer surface is irradiated by vuv photons associated with thermal annealing using the heater, the heat flow is predominantly from the front surface to the backside of the wafer. In this case the relation $T_s'=T_c'+\delta T$ is satisfied, where T_s' and T_c' are front and backside surface temperatures under vuv irradiation. The effective temperature of the near-surface region, which the UV light can penetrate, can be defined by the imaginary part of the dielectric function ($\langle\varepsilon\rangle=\langle\varepsilon_1\rangle+i\langle\varepsilon_2\rangle$) of Si(100), because increasing the phonon population rises the apparent absorption level below 3 eV. Plotted in Fig. 1 are a series of $\langle\varepsilon_2\rangle$ spectra obtained under vuv irradiation at $I_R=430$, 400, 350, and 290 mA while keeping $T_c'=300\,°C$ by setting the heater power appropriately. The $\langle\varepsilon_2\rangle$ spectra curves obtained at $T_c=450$, 500, and 550 °C by heater annealing alone are also shown by solid curves. It is evident that all $\langle\varepsilon_2\rangle$ spectra curves obtained at $T_c'=300\,°C$ are around the curve for $T_c=500\,°C$.

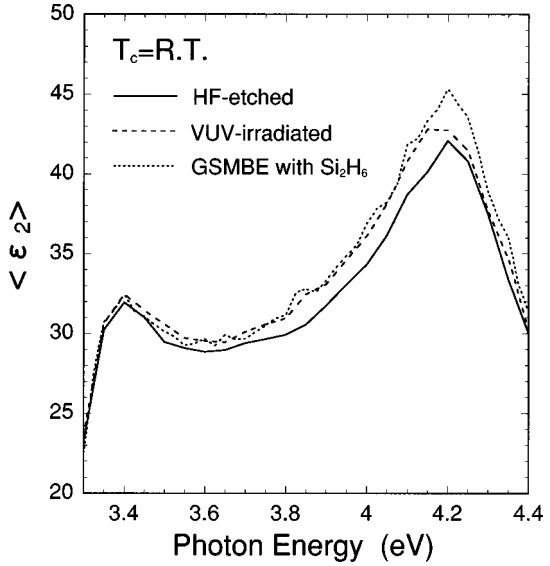

FIG. 2. Room-temperature $\langle\varepsilon\rangle$ spectra of Si(100) after HF treatment, after vuv irradiation, and after Si buffer layer growth.

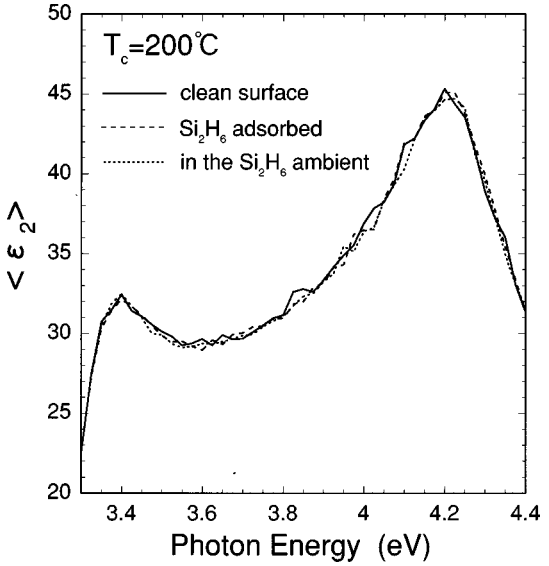

FIG. 3. $\langle\varepsilon_2\rangle$ spectra obtained from variously treated Si(100) substrate surfaces.

This kind of analysis confirmed that T_s' differed less than 60 °C between the highest and lowest vuv fluxes investigated in the present work. All SR-CVD growth reported in this paper was conducted at $T_c' = 300\,^{\circ}\mathrm{C}$, which means that T_s' was between 350 and 410 °C.

III. RESULTS

A. Formation and decomposition of $m\mathrm{SiH}_x(a)$

Prior to kinetic monitoring of SR-CVD growth with SE, the Si substrate was characterized, and the optical constant change responsible for reactive sticking of Si_2H_6 was evaluated. The imaginary part of the room temperature dielectric function of the HF-treated Si(100) substrate is shown in Fig. 2. The E_1 (3.4 eV) and E_2 (4.25 eV) critical-point features are characteristic of c-Si. Since HF etching increases the surface roughness and terminates the surface with hydrides, the E_2 amplitude is lower than 42. Subsequent vuv irradiation at $T_c' = 300\,^{\circ}\mathrm{C}$ and a Si buffer layer growth by Si_2H_6 GSMBE at $T_s = 600\,^{\circ}\mathrm{C}$ changed the surface state. vuv irradiation increased the E_2 peak amplitude slightly, perhaps because of PSD of H atoms and because of a surface flattening effect due to the migration of Si atoms. When the surface was covered by a 60-nm-thick Si buffer layer, the E_2 peak amplitude increased further, to 45, which is a similar E_2 peak amplitude to that reported for atomically clean and flat Si(100) surfaces.[14] This buffer layer was used as the standard substrate surface for SR-CVD growth in this work.

Figure 3 illustrates the interaction of Si_2H_6 with Si(100) in terms of the $\langle\varepsilon_2\rangle$ spectra. The three spectra were obtained at $T_c = 200\,^{\circ}\mathrm{C}$ from a Si(100) surface with a buffer overlayer grown by GSMBE, from a surface exposed to 10^6-L Si_2H_6 (2×10^{-3} Torr$\times$500 s) and then quickly evacuated to 1×10^{-8} Torr, and from a surface in the Si_2H_6 ambient at 2×10^{-3} Torr. The three spectra, however, are virtually the same. Repeating the same measurement with different wafers and at other temperature ($T_c = 300$ and 400 °C) revealed that any changes in the $\langle\varepsilon_2\rangle$ spectra were too small to be detected by phase-modulated SE, the noise level of which is higher than that of other type of SE optics (such as the optics using a rotating-polarizer).

When a Si(100) surface is exposed to Si_2H_6 gas and vuv photons simultaneously, however, the situation differs from one in which the only processes are thermal. Figure 4 depicts a mass spectrum of positive ions resulting from photolysis of Si_2H_6. The spectrum features are somewhat distinct from those measured on beamline 1C at the Photon Factory (Fig. 2 in Ref. 2): in Fig. 4 signals from doubly excited ions (SiH_x^{2+}) appear in addition to signals from H^+, H_2^+, SiH_x^+ ($x=0-2$), and $Si_2H_y^+$ ($y=0-6$). The eight times higher total photon flux on beamline 7 is responsible for reionization of singly charged ions. There is three times as much SiH_x^+ as $Si_2H_y^+$. These Si-containing products are sources of Si atoms supplied to the surface.

Figure 5 shows how the $\langle\varepsilon\rangle$ spectrum undergoes change resulting from two cycles of Si_2H_6 exposure and evacuation.

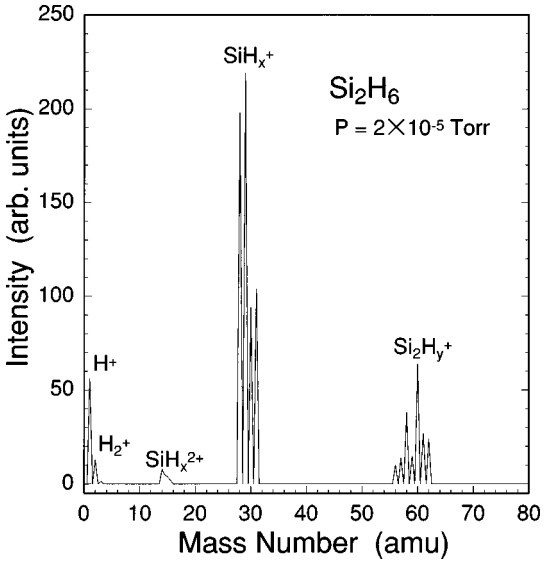

FIG. 4. Mass spectrum of positive ions produced from photolysis of Si_2H_6 at 2×10^{-5} Torr.

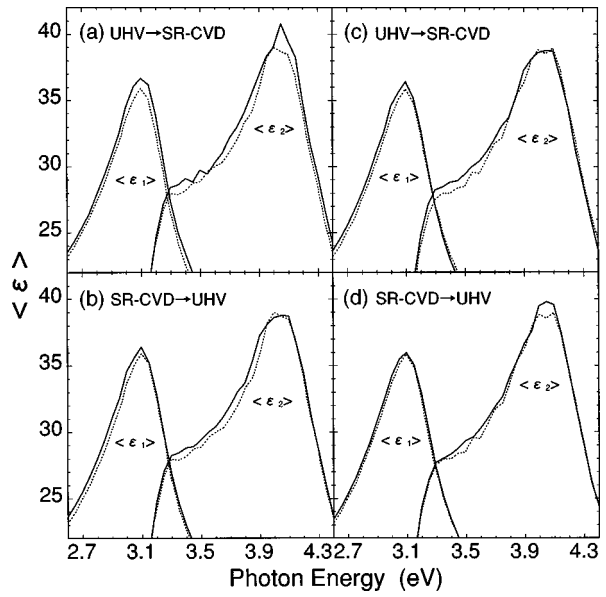

FIG. 5. Four sets of $\langle\varepsilon\rangle$ spectra obtained from surfaces subjected to vuv irradiation both under UHV (solid curves) and when exposed to Si_2H_6 (dotted curves).

Measurement was done at an appropriate vuv flux, so that the optical constant of the Si overlayer became stationary. The corresponding situation in the real space is that the epitaxial crystallinity and surface roughness was kept intact, irrespective of increasing the film thickness. The four sets of $\langle\varepsilon_2\rangle$ spectra show that the peak amplitudes at the E_1 and E_2 critical-point energies decreased when the surface was exposed to Si_2H_6 gas, and that they recovered the initial level when the gas was evacuated. It was confirmed in a control experiment that the room-temperature $\langle\varepsilon\rangle$ spectrum was entirely the same before and after vuv irradiation of the buffer Si layer. Since the generation of radicals and ions in the ambient does not itself affect the angles Ψ and Δ, the changes in the optical response must have been due to the interaction of the photolysis products with the surface. A reasonable explanation for these changes is that a transient $m\mathrm{SiH}_x(a)$ layer more than a monolayer thick produced optical contrast with the underlying Si crystal, and this layer can exist only when Si_2H_6 is supplied.

B. Photon-flux-dependent $\Psi-\Delta$ trajectories

The distinct crystallinty of Si films depending on vuv photon flux has recently been shown by the combined study with SE and XTEM.[7] The growth modes inferred from the kinetic SE data can be categorized into three groups schematically illustrated in Fig. 6. The absolute vuv flux when each growth type manifests itself is changed by Si_2H_6 pressure (deposition rate), temperature, and the initial condition of the substrate surface. The figure was drawn under the assumption that the Si_2H_6 pressure was 3×10^{-3} Torr, T_c' was 300 °C, and the Si(100) substrate was with a Si buffer layer. Numbers of growth experiments showed that when T_c' was between 220 and 320 °C (corresponding to a T_s' between 300 and 400 °C) the crystallinity depended little on T_s but much more on the vuv flux. During type-II growth the epitaxy is maintained, but is accompanied by the building up of

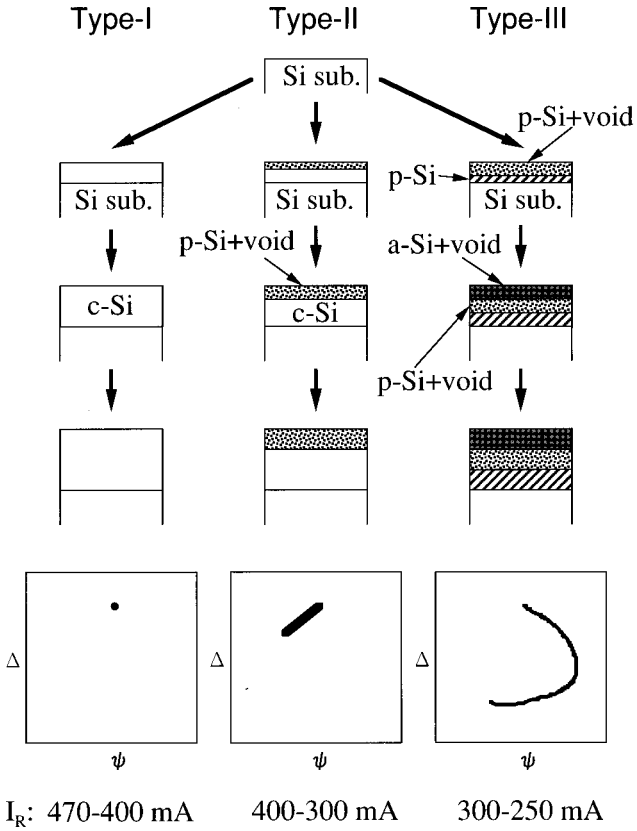

FIG. 6. Three types of vuv flux-dependent growth modes and corresponding $\Psi-\Delta$ plots (the photon energy is 3.4 eV).

a voild-containing polycrystalline Si ($p-$Si) network on the growing surface. During type-III growth, however, the epitaxy is terminated halfway. It is worth noting that even at the beginning of growth the growth modes can be judged because the directions of the traces in the $\Psi-\Delta$ plot for type-II and -III growths are clearly distinctive.

Figure 7 depicts $\Psi-\Delta$ trajectories produced by intermittent Si_2H_6 exposure and evacuation under large vuv fluxes ($I_R=420-370$ mA). These trajectories, confined to a range never far from the start point ($\Psi=22.9°\pm0.2°$ and $\Delta=151.7°\pm0.7°$), indicate type-I growth. Correspondingly, the $\langle\varepsilon\rangle$ spectra measured during the intervals of between successive growth steps are actually degenerated, as shown in Fig. 8. This indicates that the epitaxial crystallinity was maintained throughout the repeated growth cycles. Si adatoms deposited are incorporated in the Si crystal network instantly without causing any optical interference between the c-Si substrate.

In the first round of growth (GR1) the (Ψ,Δ) point moved to the left (trace $A\rightarrow B$) immediately after the beginning of the Si_2H_6 exposure at 1×10^{-3} Torr. The time for this part of the trajectory was 10–20 s, whereas the Si_2H_6 pressure stabilized within 3 s of when the gas injection started. The longer time needed for the SE signal to settle indicates that the change in the Ψ angle ($|\delta\Psi|\simeq0.2°$) is caused not by the presence of ambient Si_2H_6 gas but by surface passivation with $m\mathrm{SiH}_x(a)$. We confirmed that starting and stopping the Si_2H_6 gas exposure in the absence of the vuv beam does not produce (Ψ,Δ) angle changes of a similar scale ($|\delta\Psi|<0.025°$). This is also evident from the identity of the $\langle\varepsilon\rangle$ spectra shown in Fig. 3.

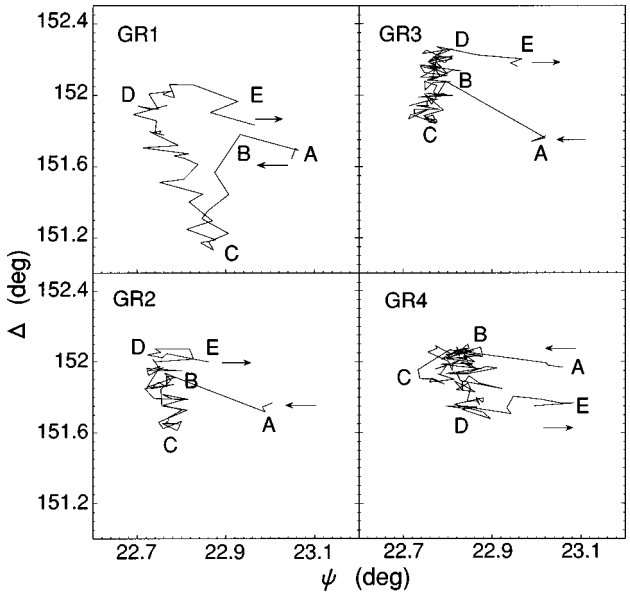

FIG. 7. $\Psi-\Delta$ plot representing the type-I growth resulting from four cycles of Si_2H_6 exposure and evacuation. The ring current decayed from 420 to 370 mA during the growth, and the Si_2H_6 pressure was 1×10^{-3} Torr. The growth times for $GR1$, $GR2$, $GR3$, and $GR4$ were 7, 7, 14, and 14 min, respectively.

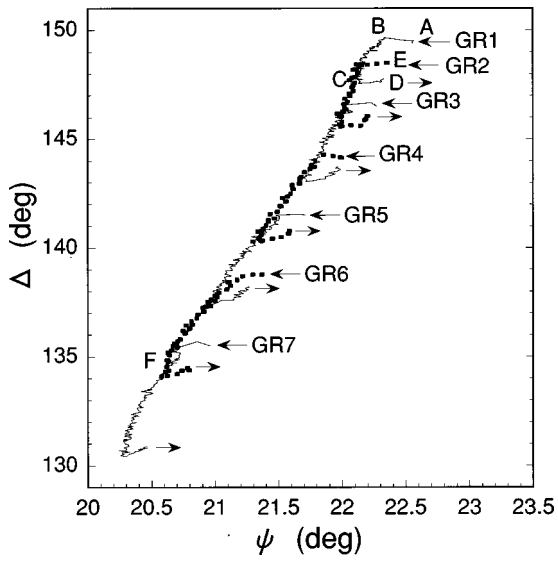

FIG. 9. $\Psi-\Delta$ plot representing the type-II growth occurring during seven 15-min cycles of Si_2H_6 exposure and evacuation. For clarity the trajectories denoted by odd numbers are plotted as thin solid lines, and the trajectories denoted by even numbers are plotted as dotted lines. The ring current decayed from 370 to 280 mA during these seven cycles, and the Si_2H_6 pressure was 3×10^{-3} Torr.

During steady-state growth, the (Ψ,Δ) point first moved downward slightly (trace $B\rightarrow C$) and then upward (trace $C\rightarrow D$) again. The Si film growth rate was 0.36 nm min^{-1}, and a film 2.5 nm thick was grown during the time the point moved from B to D. These observations suggests that the surface roughness initially increased as two-dimensional Si island nucleated over the surface, but became flat again when the islands coalesced into large domains. Similar closed-loop trajectories were observed by Li *et al.*[15] during Si_2H_6 GSMBE at 600–700 °C.

When the Si_2H_6 gas was evacuated, the (Ψ,Δ) point moved immediately to the right (trace $D\rightarrow E$) corresponding to the disappearance of $m\mathrm{SiH}_x(a)$. We emphasize here that the instantaneous trajectory resulting from turning the Si_2H_6 supply on and off is primarily in the Ψ direction, whereas the trajectory during the bulk of a Si film growth is primarily in the Δ direction. Thus the formation of $m\mathrm{SiH}_x(a)$ can be clearly distinguished from the bulk Si growth.

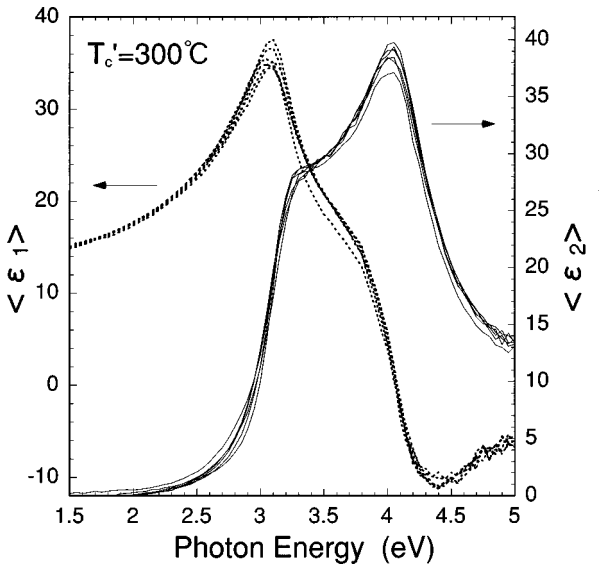

FIG. 8. Evolution of the real (dotted curves) and imaginary (solid curves) parts of the $\langle\varepsilon\rangle$ spectra corresponding to the growth shown in Fig. 7.

For the second and third rounds of growth (GR2 and GR3) the changes in (Ψ,Δ) angles were similar to those in GR1. From GR1 to GR3, however, the Δ coordinate of the end point E increases. A larger Δ in this system is equivalent to a higher E_1 peak amplitude in the $\langle\varepsilon_2\rangle$ spectrum, so this increase reflects the improvement of the flatness and/or crystallinity of the Si overlayer. SR-CVD under a high vuv flux therefore can be used to grow a Si buffer layer for the subsequent epitaxy process. For GR4 the Δ coordinate of the end point E was smaller than that of the start point A. From GR1 to GR4 the ring current decayed from 420 to 370 mA. The observation of increase (GR1, GR2, and GR3) and decrease (GR4) in the Δ coordinate means that both improvement and degradation in the crystallinity and/or surface flatness are possible as a result of SR-CVD. It is seen that the efficiency of recrystallization near the threshold storage current depends very much on the vuv flux.

Figure 9 depicts a type-II trajectory resulting from intermittent Si_2H_6 exposure under irradiation with a medium flux of vuv photons. In each cycle a 16-nm-thick Si film was grown. In GR1, as in Fig. 7, the (Ψ,Δ) point moved immediately to the left when the Si_2H_6 was introduced (trace $A\rightarrow B$), and moved immediately to the right when the Si_2H_6 was evacuated (trace $C\rightarrow D$). The lengths of these two vectors are the same but their directions are opposite. The lengths ($|\delta\Psi|\simeq0.2°$) are also similar to the lengths of the corresponding vectors in Fig. 7, even though the Si_2H_6 pressure differed by a factor of 3 between the experimental conditions used to gather the data shown in the two figures. This

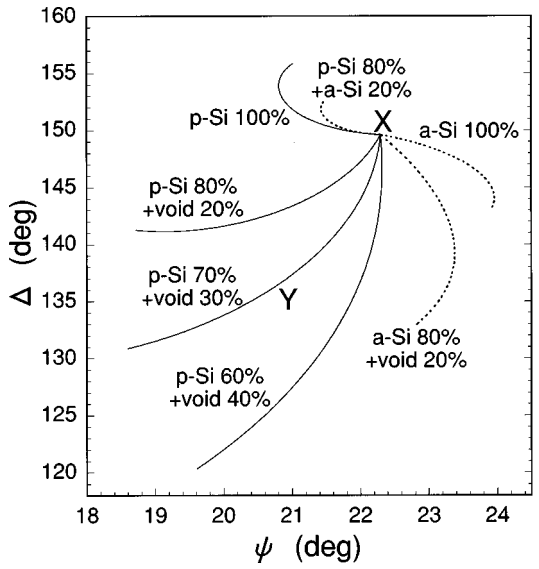

FIG. 10. Simulated type-II trajectories for various overlayer compositions. In each trace the overlayer thickness at the end point is 10 nm. The envelope line *B*-*C*-*F* of the experimental trajectories in Fig. 9 is best fitted by the trajectory for *p*-Si (70%) plus void (30%).

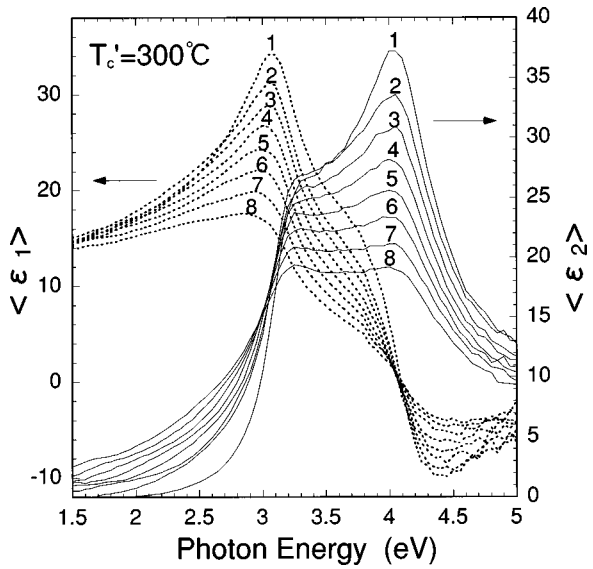

FIG. 11. Evolution of the real (dotted curve) and imaginary (solid curves) parts of the $\langle\varepsilon\rangle$ spectrum corresponding to the growth shown in Fig. 9. The numbers indicate the order in which the spectra were measured.

similarity indicates that the thickness of the Si hydride passivation layer is self-limited. The envelope line of the traces during the stationary growth (line *B*-*C*-*F*), on the other hand, indicates the deposition of a Si-Si network with a crystallinity different from that of *c*-Si. This deposition produced optical contrast between the substrate Si medium.

Figure 10 shows trajectories simulated assuming a uniform deposition of films of various compositions. The trajectories extend radially from the start point *X* (corresponding to the point *B* in Fig. 9), and their directions are determined by the composition of the material. The directions of the trajectories for *a*-Si (100%), *a*-Si (80%) plus void (20%), *p*-Si (100%), and *p*-Si (80%) plus *a*-Si (20%) deposition differ even qualitatively from that of the *B*-*C*-*F* line in Fig. 9. The best-fit result was obtained by the trajectory for the *p*-Si (70%) plus void (30%) component, which is denoted (-SiH_x-) in scheme (1). Figure 11 is a summary of the $\langle\varepsilon\rangle$ spectra measured during the intervals between successive growth steps. The E_1 and E_2 peak amplitude gradually decreased as the thickness of the film increased, while the E_1 and E_2 critical point features were conserved. The reduction in amplitude is consistent with the buildup of a void-containing crystalline Si overlayer. As Ψ in Fig. 9 varied from 22.5° to 21°, a Si film 80 nm thick was grown, but the thickness of the overlayer at the point *X* in Fig. 10 is only 5 nm. This disagreement indicates that, like $m\mathrm{SiH}_x(a)$, that forms and decomposes, a void-rich Si overlayer (-SiH_x-) is continuously forms from $m\mathrm{SiH}_x(a)$ and is converted to *c*-Si during SR-CVD. Such a dynamical process can also be inferred from the discrepancy between the end point *D* when the Si_2H_6 supply is stopped and the start point *E* of the next growth cycle in Fig. 9. Obviously, the void layer was recrystallized during the time that the Si_2H_6 supply was turned off. Recrystallization occurs throughout the growth process, and if it does not keep up with the supply of Si atoms, a void-containing network gradually builds up.

Figure 12 shows type-III trajectories resulting from five cycles of growth process under a small vuv flux. The longer trajectory, compared with those in Figs. 7 and 9, indicates the more greatly deteriorating crystallinity from *c*-Si to *a*-Si.

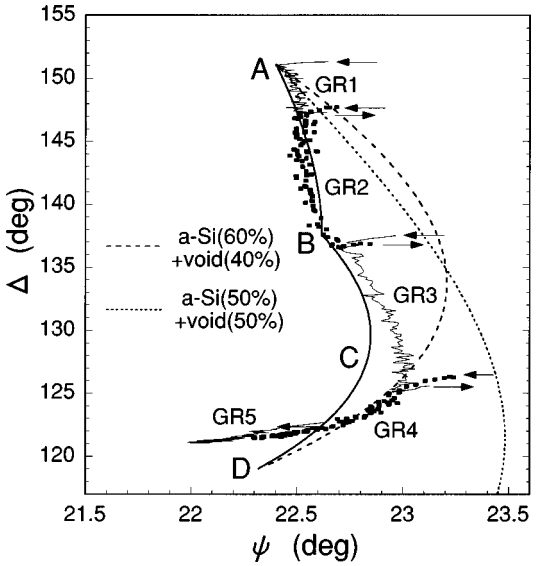

FIG. 12. $\Psi-\Delta$ plot representing the type-III growth resulting from five 15-min cycles of Si_2H_6 exposure and evacuation. For clarity the trajectories denoted by odd numbers are plotted as thin solid lines, and the trajectories denoted by even numbers are plotted as dotted lines. The ring current decayed from 290 to 270 mA during the five cycles, and the Si_2H_6 pressure was 3×10^{-3} Torr. The broken lines are a simulated trajectory obtained by assuming the buildup of an *a*-Si (60%) plus void (40%) layer, and that obtained assuming the buildup of an *a*-Si (50%) plus void (50%) layer from the *c*-Si interface. The thick solid line is a simulated trajectory obtained assuming the deposition of a 3.3-nm-thick *p*-Si (50%) plus void (50%) layer (trace $A\rightarrow B$) followed by deposition of a 7.5-nm-thick *a*-Si (60%) plus void (40%) overlayer (trace $B\rightarrow C\rightarrow D$).

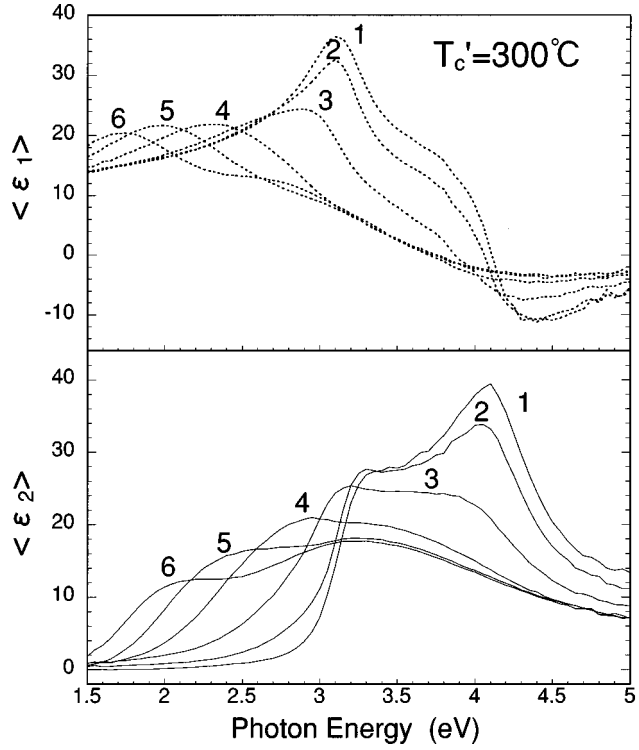

FIG. 13. Evolution of the real (dotted curves) and imaginary (solid curves) parts of the $\langle\varepsilon\rangle$ spectrum corresponding to the growth shown in Fig. 12. The numbers indicate the order in which the spectra were measured.

Another notable difference is that the trajectories are arranged consecutively without overlapping one another. This suggests that the crystallinity was not affected at all by the small vuv flux during the spectrum measurement time and that crystallization stimulated by vuv photons is necessary if low-temperature epitaxy is to be maintained. Once a closely packed, disordered Si layer is deposited, it is resistant to restructuring because a very high activation barrier must be overcome if Si atoms in a densified film are to be displaced. The simulation curve fitted to the experimental trajectories was obtained by assuming deposition of a 3.3-nm-thick p-Si (50%) plus void (50%) layer (trace $A\rightarrow B$) followed by deposition of a 7.5-nm-thick a-Si (60%) plus void (40%) overlayer (trace $B\rightarrow C\rightarrow D$). Neither the trajectory obtained assuming the buildup of an a-Si (60%) plus void (40%) layer nor that obtained assuming the buildup of an a-Si (50%) plus void (50%) layer from the c-Si interface failed to reproduce the experimental trajectories.

As seen from Fig. 13, the shape of the $\langle\varepsilon\rangle$ spectrum measured at intervals throughout the Si_2H_6 exposure time changed quickly. The E_1 and E_2 critical-point features were absent after GR3, and were replaced by a single broad peak centered at 3.3 eV, reflecting the deposition of an amorphouslike overlayer.[16] A shift in the growth mode from type II to type III occurs when imperfections such as point defects and stacking faults involving higher-order hydrides begin to accumulate at a rate greater than that at which they can be repaired and the network kept crystalline.

C. Recrystallization of Si films

Figure 14 depicts an example of the overall trajectory during growth and after the Si_2H_6 supply was stopped, highlighting the post-irradiation effect of vuv photons. The substrate for this growth was the HF-treated Si (100) without a buffer layer. Trace $A\rightarrow B$ again corresponds to the formation of a $m\mathrm{SiH}_x(a)$ layer. From point B to point E the trajectory was that of type-III growth because the initial surface was rough, and just when the amorphous phase was going to nucleate (at point E), the Si_2H_6 supply was turned off. Trace $E\rightarrow F$, which corresponds to the disappearance of $m\mathrm{SiH}_x(a)$, took 50 s. During the continuing irradiation the (Ψ,Δ) point moved from F to G, and this movement was much slower than that corresponding to the prompt decomposition of $m\mathrm{SiH}_x(a)$. Because trace $F\rightarrow G$ is almost parallel to the growth trace $C\rightarrow D\rightarrow E$, it evidently reflects a process that is the reverse process but without the $m\mathrm{SiH}_x(a)$ layer. That is, the nominal thickness of the Si overlayer with inferior crystallinity decreased gradually. Hence, what occurred during the trace $F\rightarrow G$ was the solid-phase epitaxy of a Si film overlayered on the epitaxial Si film. Numbers of measurement of the $\langle\varepsilon\rangle$ spectra before and after post-irradiation confirmed the recrystallization. For such recrystallization to occur after a few hundred Å of Si are grown, the storage current must be more than 400 mA when the Si_2H_6 supply is shut off.

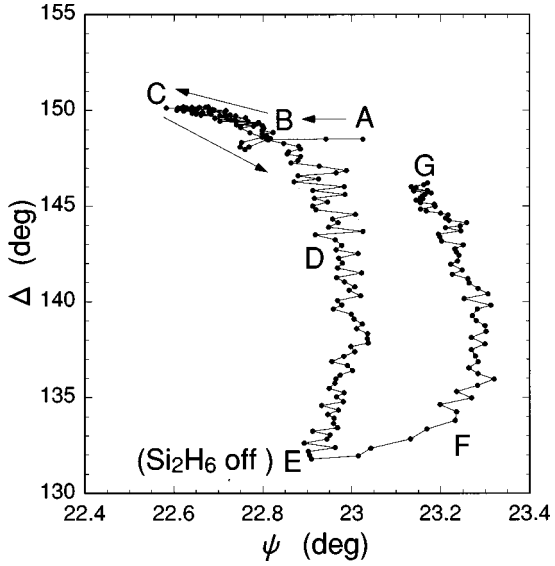

FIG. 14. $\Psi-\Delta$ plot for a 30-nm-thick Si film grown on a HF-treated surface by SR-CVD (trace $A\rightarrow B\rightarrow C\rightarrow D\rightarrow E$) and continued irradiation (trace $E\rightarrow F\rightarrow G$). The ring current was between 430 and 400 mA.

Figure 15 shows a trajectory obtained during SR-CVD (trace $A\rightarrow B\rightarrow C\rightarrow D\rightarrow E$) and post-irradiation (trace $E\rightarrow F\rightarrow G$) when using a buffer-Si-grown substrate. Its shape differs from that of the trajectory in Fig. 14 because of the different growth history due to the different initial surface roughness. Trace $C\rightarrow D$ indicates type-II growth, and the growth of the epitaxial Si film was accompanied by the buildup of a void-containing Si layer. At point D the direction of the trajectory changed, indicating the onset of disordered network nucleation. When the Si_2H_6 supply was shut off at point E, the $m\mathrm{SiH}_x(a)$ layer decomposed within 40 s (trace $E\rightarrow F$). After that the trajectory was directed toward the start point by post-irradiation (trace $F\rightarrow G$).

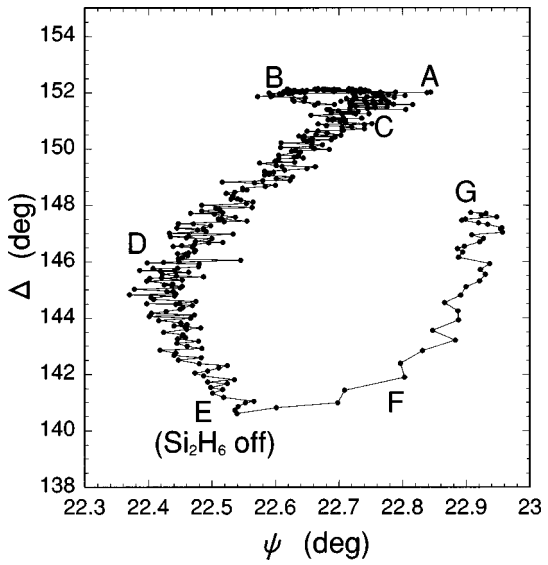

FIG. 15. $\Psi-\Delta$ plot for an 80-nm-thick Si film grown on a Si-buffer layer by SR-CVD (trace $A\rightarrow B\rightarrow C\rightarrow D\rightarrow E$) and irradiation continued (trace $E\rightarrow F\rightarrow G$). The ring current was between 450 and 390 mA.

When the network restructuring was completed, however, the end points *G* in Figs. 14 and 15 were not at the start point which defines the optical constant of *c*-Si. Either the crystallinity of the film is inferior to that of the substrate, or the surface of the film is rougher than that of the substrate, or both. When voids in the as-deposited film disappear, the film shrinks and has an inhomogeneous distribution of defects as well as microscopic surface roughness. For the thickness uniformity of an atomic order to be maintained, there must be a mechanism for flattening the surface. In GSMBE conducted at high temperatures, for example, Si adatom migration reduces the microscopic roughness, and layer-by-layer growth can therefore be achieved.

How the radiation effect contributes to recrystallization was investigated by changing growth parameters during the type-II growth (the transition regime between type-I and -III growths). Consider first the effect of growth rate. The results of about 50 growth experiments confirmed that epitaxial growth was maintained longer at lower Si_2H_6 pressures. For a given ring current, the crystallinity of a film grown at 1×10^{-3} Torr for 20 min, for instance, is superior to that of a film grown at 2×10^{-3} Torr for 10 min. At pressures between 10^{-3} and 10^{-2} Torr the SR-CVD growth rate is proportional to Si_2H_6 pressure,[2] but the PSD rate is in principle independent of Si_2H_6 pressure. We therefore compare the crystallinities of films of the same thickness. In the former case (10^{-3} Torr for 20 min), twice as much time is available for PSD to remove H atoms and for a Si-Si network to be formed. The results of these experiments support the contention that vuv irradiation prevents the growth of a hydrogenated amorphous network. If the rates of H removal and surface flattening are insufficient, the amount of H atoms incorporated greatly exceeds the solubility limit, and these atoms become a source of lattice imperfections and degrade crystallinity. If SiH_x radicals are supplied slowly, there is enough time for H atoms to be removed from the surface and for Si adatoms to migrate to the exact crystal nucleation sites.

Now consider the effect of vuv flux. For crystallization in the bulk network, we expect the vuv flux to be more important than the irradiation time. This means that if the vuv flux is not sufficient, even prolonged irradiation may improve the crystallinity very little. It was found, for example, that the crystallinity of a film grown at $I_R=450$ mA and $P=3\times10^{-3}$ Torr was superior to that of one grown at $I_R=300$ mA and $P=2\times10^{-3}$ Torr. In the high-current case, the rate at which SiH_x radicals are supplied and the rate of H removal by PSD are 1.5 times higher than they are in the low-current case. We note that T_s' differs by only 50 °C between the high and low storage currents, while the power density of photons delivered in the film differs by a factor of 1.5. This indicates that the photochemical reaction is initiated 1.5 times more frequently in the high-current case. The crystallization being dominated by the vuv flux suggests that Si-Si network rearrangement at the *c*-Si interface throughout the growth process is important for maintaining epitaxy.

IV. DISCUSSION

A. Dynamical processes in the ambient and at the outermost surface

The dissociative chemisorption of Si_2H_6 on Si (100) proceeds according to the following established schemes.[17,18]

$$Si_2H_6(g)\rightarrow Si_2H_6(a), \tag{2}$$

$$Si_2H_6(a)+2\_\rightarrow 2SiH_3(a), \tag{3}$$

$$SiH_3(a)+\_\rightarrow SiH_2(a)+H(a), \tag{4}$$

where (g) and (a), respectively, designate gas and adsorbate, and where _ is a dangling-bond-terminated surface site. If all dangling bonds are consumed, the saturated surface would hypothetrically be covered by a half-monolayer of monohydride $[H(a)]$ and a half-monolayer of dihydride $[SiH_2(a)]$. However it is not, because steric hinderance prevents Si_2H_6 molecules from reaching the sites available for dissociation. The extremely small change in the optical constant (see Fig. 3) indicates that the coverage of $SiH_x(a)$ is far below the submonolayer level.

The prompt increase and decrease in Ψ value that are associated with Si_2H_6 exposure and evacuation under vuv irradiation are evidence of the formation and decomposition of a transient $mSiH_x(a)$ multilayer. Concerning the decomposition mechanism, recombinative H_2 desorption from hydrides by a thermal mechanism can be ruled out because a desorption rate comparable to that observed in the present study would be obtained only at T_s' above 500 °C. A photochemical mechanism is therefore likely. Few of the SiH_x admolecules will be removed as result of electronic excitation rupturing entirely covalent Si-SiH_x bonds. The most probable decomposition pathway is PSD of H from $mSiH_x(a)$. Time-of-flight mass spectroscopy using single-bunch operation of a synchrotron radiation ring has in fact shown that H^+ is the primary desorption product obtained from Si surfaces and that Si-containing ions such as SiH_x^+ and $Si_2H_y^+$ are never observed.[19] Observation of the surface structure with reflection high-energy electron diffraction revealed that an atomically flat Si (100) surface is conserved

even after vuv irradiation.[20] This suggests that the damage on the flat Si surface is negligible. The resultant Si adatoms having dangling bonds may be incorporated as constituents in the Si-Si crystal network and cannot be optically discriminated from the substrate Si atoms. Thus $m\mathrm{SiH}_x(a)$ is an intermediate state between photolysis products and a Si network.

The thickness of the $m\mathrm{SiH}_x(a)$ layer under conditions of creation-annihilation equilibrium can be estimated from the $\langle\varepsilon\rangle$ spectra. The relation between $\langle\varepsilon\rangle$ and the substrate dielectric function (ε_s) of an overlayer with thickness d is given by $\langle\varepsilon\rangle \simeq \varepsilon_s + 4\pi i d {\varepsilon_s}^{3/2}\lambda^{-1}$, where λ is the wavelength of the light.[21] This relation is valid when the amplitude of the overlayer dielectric function is much smaller than $|\varepsilon_s|$. Applying this formula near the E_1 energy in Fig. 5 yields $d \simeq 0.3$ nm. The difference between the optical properties of $m\mathrm{SiH}_x(a)$ and c-Si can be ascribed to the intrinsic optical response of Si-H bonds.[22,23] Most of the H atoms bonded to Si hydrides, however, are not eventually incorporated in the Si crystal. Measurement by secondary-ion-mass spectroscopy has in fact revealed that the concentration of H atoms in the Si film is 10^{20}–10^{21} cm^{-3}.[24] This indicates that the Si atoms making up the crystal network are those deprived of H atoms, and that the H atoms included in the Si crystal are restricted to grain boundaries or point defects.

The passivation of the surface by higher-order hydrides was also inferred from the growth kinetics of silane plasma-enhanced chemical-vapor deposition (PECVD). Miyazaki *et al.*[25] confirmed by Fourier-transform infrared spectroscopy that the predominant surface species during silane PECVD is a polysilane consisting of $(\mathrm{SiH}_2)_n$ chains terminated by SiH_3. The other available evidence is that exposing the growing surface with silicon hydride radicals and atomic hydrogen alternately facilitates layer-by-layer deposition of a μc-Si film at temperatures as low as 250 °C.[26,27] This can be interpreted as indicating that higher-order Si hydrides like SiH_3 can be removed by reacting with atomic H to form a stable SiH_4 molecule and are thus not destined to contribute to epitaxy. Monohydrides and dihydrides bound to substrate atoms by two or three backbonds, on the other hand, are stable species resistant to attack by atomic H and are readily incorporated into the film. Therefore most of the surface under steady-state growth conditions is passivated by higher-order hydrides.

B. Network restructuring in the near-surface region

For the $m\mathrm{SiH}_x(a)$ multilayer to be transformed into a Si film, the Si admolecules or chains must become chemically bonded to one another. The representative effect occurring at the surface irradiated by vuv photons is PSD. Slightly ionic Si-H bonds are efficiently broken by the direct Auger-stimulated desorption initiated by core electronic excitation.[28] The H is then ejected into the ambient, regenerating a dangling-bond-terminated site ($\cdot\mathrm{SiH}_{x-1}$):

$$\text{-}\mathrm{SiH}_x + h\nu \rightarrow \text{-}\mathrm{SiH}_{x-1}\cdot + \mathrm{H}(\mathrm{H}^+). \tag{5}$$

This H removal process increases the growth rate by producing vacant sites that can accept incoming SiH_x radicals and by triggering bonding between the SiH_x species. Epitaxy is also promoted by the consequent weakening of the hydrogen surfactant effect that suppresses the migration of adatoms. Incorporation of excess H atoms bonded to dihydrides or trihydrides into the bulk is detrimental to the crystal growth.[29]

Although PSD is usually treated as a surface phenomenon, its mechanism is also relevant to the electronically excited bond-breaking processes occurring inside the bulk material,[30] i.e., reaction (5) can be applied to near-surface H-terminated Si-Si network. The total cross section of PSD involving all Si-H bonds in the Si-Si network is substantial. If the temperature is high enough, the H atoms ejected into interstitial spaces can migrate into the bulk. When two H atoms encounter one another, they can recombine and desorb as H_2 from the surface. The dangling-bond-terminated branch of the network ($\text{-}\mathrm{SiH}_{x-1}\cdot$), on the other hand, will seek for a new bonding partner to reduce its free energy. The vibrational motion of these chains enhances their mutual interaction and facilitates substitutional reactions leading to networking:

$$\text{-}\mathrm{SiH}_{x-1}\cdot + \text{-}\mathrm{SiH}_y \rightarrow \text{-}\mathrm{SiH}_{x-1}\text{-}\mathrm{SiH}_{y-1} + \mathrm{H}. \tag{6}$$

If the two chains are located in nearest-neighbor positions, their overall reaction can be expressed by

$$\text{-}\mathrm{SiH}_x + \text{-}\mathrm{SiH}_y + h\nu \rightarrow \text{-}\mathrm{SiH}_{x-1}\text{-}\mathrm{SiH}_{y-1} + \mathrm{H}_2. \tag{7}$$

This scheme, involving H-H bond formation, has a low-energy cost.[31] In fact, when an a-Si:H film was irradiated with vuv photons, strong H_2 desorption was observed even at $T_c' = 100$ °C. Similar low-temperature H_2 desorption has been observed when SiN_x:H films are irradiated with vuv photons.[32] The combined reactions (5) and (6) or reaction (7) will therefore trigger the nonthermal networking of Si admolecules.

C. Microscopic processes for vuv-induced recrystallization

As identified by the formation of the $m\mathrm{SiH}_x(a)$ layer, Si epitaxy by SR-CVD proceeds by a multilayer mode rather than in a layer-by-layer manner. Since the random making of bonds between Si hydride admolecules or $(\mathrm{SiH}_2)_n$ chains contained in $m\mathrm{SiH}_x(a)$ does not necessarily produce a Si epilayer, a certain mechanism must serve to rearrange the random network into an ordered Si crystal lattice. Although a T_s greater than 650 °C is needed to induce solid-phase epitaxy by simple thermal annealing, $T_s' \leqslant 410$ °C in the present SR-CVD system.

Although Si-H bonds are easily broken through an electronic mechanism, an entirely covalent Si-Si bond is much harder to break because valence electrons nonlocalized over the network facilitate faster hopping decay of valence holes. Another reason for the stability of Si-Si bonds in the network is that two or three backbonds must be broken simultaneously if a Si atom coordinated with several Si atoms is to be displaced. Hence for a restructuring of the Si-Si network to occur, a greater number of valence holes must be localized than in the case of the Si-H bond.

The density of excited atoms, however, is too low to cause multiple photon processes. Absorption of vuv photons in the solid material occurs predominantly through the excitation of a Si($2s$) or Si($2p$) core electron. For photons with energies ranging from 100 to 300 eV (most of the vuv pho-

tons used in the present experiments), the extinction coefficient in the bulk Si is approximately 20 μm^{-1}. This means that 63% of photons are absorbed within 50 nm of the surface, a region containing 2.5×10^{15} Si atoms per 1 mm^2 surface area. Given the photon flux of $1\times10^{16}\,s^{-1}\,mm^{-2}$ at $I_R = 440$ mA, each Si atom is excited only four times per second.

When the normal Auger decay process follows, two holes are created in the valence orbital. If shake-up or shake-off ionization occurs, however, three and four holes are eventually created. From the state in which multiple holes are localized, strong Coulomb repulsion between holes causes a breaking of multiple bonds, which is referred to as a Coulombic explosion. Another possible route for the network restructuring is electron-stimulated migration (ESM) of adatoms.[33,34] The mechanism underlying ESM involves highly mobile species produced by electron attachment to adatoms. Since numerous photoelectrons, Auger electrons, and secondary electrons are emitted with absorption of vuv photons, ESM is likely to contribute. In addition to these electronic processes, ''suprathermal'' or ''hot atom'' reactions would also occur in such highly excited state.[35,36] When the valence hole is quenched by electron-hole recombination, a potential energy higher than a few eV is released. The energy is imparted to nearby atoms, and this is equivalent to very local heating. The energy transfer from these hot atoms to the surrounding atoms may cause suprathermal bond-exchange processes.

Figure 16 shows a model of the structure of the outermost surface and near-surface region during SR-CVD. From the ambient to the substrate, the layers consist of Si_2H_6 molecules and photolysis products such as SiH_x and Si_2H_y, $m\mathrm{SiH}_x(a)$ at the outermost surface, a near-surface network of $(\text{-SiH}_x\text{-})$, and a Si epilayer. The growth pathway is summarized as follows. The reaction is initiated by photolysis of Si_2H_6 both in the gas phase and at the surface. The SiH_x radicals impinge on the surface and form a $m\mathrm{SiH}_x(a)$ passivation layer. At this stage the SiH_x fragments in $m\mathrm{SiH}_x(a)$ are not bound to one another. vuv impact stimulates bonding between these fragments and results in the formation of a void-containing crystalline network. This network is further transformed into a compact Si crystal by vuv-stimulated bond-rearrangement processes.

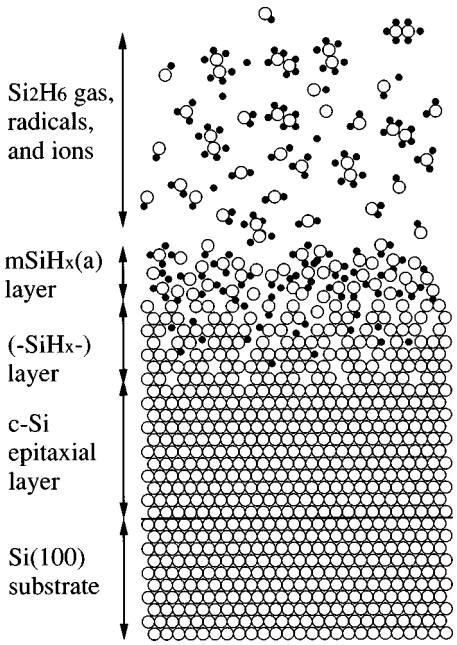

FIG. 16. Structural model of type-II Si growth on Si (100).

V. CONCLUSION

Spectroellipsometric measurement during SR-CVD verified that scheme (1) accounts for the conversion of photolysis products of Si_2H_6 into a Si epitaxial film. At the outermost surface there is a precursor state leading to networking: when the Si surface is exposed to Si_2H_6 under vuv irradiation, a $m\mathrm{SiH}_x(a)$ layer is created quickly. When the gas is evacuated, this layer promptly decomposes by PSD of H atoms. During the steady-state growth, three vuv flux-dependent growth modes have been identified. They are characterized by the evolution of dielectric function change and can be distinguished by differences in the (Ψ,Δ) trajectories. When the vuv flux is sufficiently large, the Si adatoms are instantaneously incorporated into the network of the Si epitaxial layer, and the dielectric function of c-Si is maintained. When a smaller vuv flux is applied, both Ψ and Δ angles decrease as a result of the building up of a crystalline network including voids. The deposition rate higher than the recrystallization rate is responsible for the formation of this $(\text{-SiH}_x\text{-})$ layer. The transient formation of $m\mathrm{SiH}_x(a)$ can be distinguished from the building up of the $(\text{-SiH}_x\text{-})$ layer by the direction of (Ψ,Δ) trajectories. At still smaller vuv fluxes the crystallinity deteriorates rapidly as growth proceeds. The continuous crystallization improvement due to the vuv flux is needed to maintain epitaxy. The radiation effect includes photon-stimulated desorption of H atoms that generates dangling-bond-terminated sites, and the electronically excited Si-Si network rearrangement into a crystalline network.

ACKNOWLEDGMENTS

I thank S. Matsuo for supporting this research program, and T. Hosokawa for useful discussions.

[1] H. Akazawa, M. Nagase, and Y. Utsumi, Appl. Phys. Lett. **64**, 754 (1994).
[2] H. Akazawa and Y. Utsumi, J. Appl. Phys. **78**, 2740 (1995).
[3] H. Akazawa, Appl. Surf. Sci. **106**, 211 (1996).
[4] H. Akazawa, J. Appl. Phys. **79**, 9396 (1996).
[5] F. Sato, K. Goto, and J. Chikawa, Jpn. J. Appl. Phys. **30**, L285 (1991).
[6] H. Akazawa, J. Takahashi, Y. Utsumi, I. Kawashima, and T. Urisu, Appl. Phys. Lett. **60**, 974 (1992).
[7] H. Akazawa, Appl. Phys. Lett. **70**, 3528 (1997).

[8] A. Polman, D. J. W. Mous, P. A. Stolk, W. C. Sinke, C. W. T. Bulle-Lieuwma, and D. E. W. Vandenhoudt, Appl. Phys. Lett. **55**, 1097 (1989).
[9] W. C. Sinke, A. Polman, S. Roorda, and P. A. Stolk, Appl. Surf. Sci. **43**, 128 (1989).
[10] H. Akazawa and J. Takahashi, Rev. Sci. Instrum. **69**, 265 (1998).
[11] V. A. Burrows, Y. J. Chabal, G. S. Higashi, K. Raghavachari, and S. B. Christman, Appl. Phys. Lett. **53**, 998 (1988).
[12] B. Drevillon, J. Perrin, R. Marbot, A. Violet, and J. L. Dalby, Rev. Sci. Instrum. **53**, 969 (1982).
[13] G. Jin, H. El Rhaleb, J. P. Roger, A. C. Boccara, and J. L. Stehle, Thin Solid Films **234**, 375 (1993).
[14] V. Nayar, W. Y. Leong, C. Pickering, A. J. Pidduck, R. T. Carline, and D. J. Robbins, Appl. Phys. Lett. **61**, 1304 (1992).
[15] M. Li, Y. Z. Hu, E. A. Irene, L. Liu, K. N. Christensen, and D. M. Maher, J. Vac. Sci. Technol. B **13**, 105 (1995).
[16] R. W. Collins, in *Amorphous Silicon and Related Materials* edited by H. Fritzsche (World Scientific, Singapore, 1988), p. 1003.
[17] F. Bozso and Ph. Avouris, Phys. Rev. B **38**, 3943 (1988).
[18] S. M. Gates, J. Cryst. Growth **120**, 269 (1992).
[19] H. Akazawa, Phys. Rev. B **51**, 7314 (1995); Nucl. Instrum. Methods Phys. Res. B **101**, 227 (1995).
[20] H. Akazawa and Y. Utsumi, J. Appl. Phys. **78**, 2725 (1995).
[21] D. E. Aspnes, Thin Solid Films **89**, 249 (1982).
[22] I. An, R. W. Collins, H. V. Nguyen, K. Vedam, H. S. Witham, and R. Messier, Thin Solid Films **233**, 276 (1993).
[23] H. Yao, J. A. Woollam, and S. A. Alterovitz, Appl. Phys. Lett. **62**, 3324 (1993).
[24] H. Akazawa, J. Cryst. Growth **173**, 343 (1997).
[25] S. Miyazaki, H. Shin, Y. Miyoshi, and M. Hirose, Jpn. J. Appl. Phys. **34**, 787 (1995).
[26] N. Layadi, P. Roca i Cabarrocas, B. Drevillon, and I. Solomon, Phys. Rev. B **52**, 5136 (1995).
[27] H. V. Nguyen, I. An, R. W. Collins, Y. Lu, M. Wakagi, and C. R. Wronski, Appl. Phys. Lett. **65**, 3335 (1994).
[28] D. E. Ramaker, C. T. White, and J. S. Murday, Phys. Lett. **89A**, 211 (1982).
[29] M. Copel and R. M. Tromp, Phys. Rev. Lett. **72**, 1236 (1994).
[30] D. R. Jennison, J. P. Sullivan, P. A. Schultz, M. P. Sears, and E. B. Stechel, Surf. Sci. **390**, 112 (1997).
[31] S. B. Zhang, W. B. Jackson, and D. J. Chadi, Phys. Rev. Lett. **65**, 2575 (1990).
[32] H. Akazawa, Nucl. Instrum. Methods Phys. Res. B **116**, 355 (1996).
[33] A. G. Fedorus, E. V. Klimenko, A. G. Naumovets, E. M. Zasimovich, and I. N. Zasimovich, Nucl. Instrum. Methods Phys. Res. B **101**, 207 (1995).
[34] H. J. Jansch, J. Xu, and J. T. Yates, J. Chem. Phys. **99**, 721 (1993).
[35] K. Rossler, Nucl. Instrum. Methods Phys. Res. B **65**, 55 (1992).
[36] X.-Y. Zhu, Surf. Sci. **390**, 224 (1997).